Environmental Science & Technology

Article

pubs.acs.org/est

Selective Degradation of Organic Pollutants Using an Efficient Metal-Free Catalyst Derived from Carbonized Polypyrrole via Peroxymonosulfate Activation

Peidong Hu,[†] Hanrui Su,[†] Zhenyu Chen,[†] Chunyang Yu,[‡] Qilin Li,[∥] Baoxue Zhou,[†,§] Pedro J. J. Alvarez,[∥] and Mingce Long*[,†,§]

[†]School of Environmental Science and Engineering, [‡]School of Chemistry and Chemical Engineering, and [§]Key Laboratory for Thin Film and Microfabrication of the Ministry of Education, Shanghai Jiao Tong University, Shanghai 200240, China

[∥]Department of Civil and Environmental Engineering, Rice University, Houston, Texas 77005, United States

Supporting Information

ABSTRACT: Metal-free carbonaceous materials, including nitrogen-doped graphene and carbon nanotubes, are emerging as alternative catalysts for peroxymonosulfate (PMS) activation to avoid drawbacks of conventional transition metal-containing catalysts, such as the leaching of toxic metal ions. However, these novel carbocatalysts face relatively high cost and complex syntheses, and their activation mechanisms have not been well-understood. Herein, we developed a novel nitrogen-doped carbonaceous nanosphere catalyst by carbonization of polypyrrole, which was prepared through a scalable chemical oxidative polymerization. The defective degree of carbon substrate and amount of nitrogen dopants (i.e., graphitic nitrogen) were modulated by the calcination temperature. The product carbonized at 800 °C (CPPy-F-8) exhibited the best catalytic performance for PMS activation, with 97% phenol degradation efficiency in 120 min. The catalytic system was efficient over a wide pH range (2−9), and the reaction of phenol degradation had a relatively low activation energy (18.4 ± 2.7 kJ mol^{-1}). The nitrogen-doped carbocatalyst activated PMS through a nonradical pathway. A two-step catalytic mechanism was extrapolated: the catalyst transfers electrons to PMS through active nitrogen species and becomes a metastable state of the catalyst (State I); next, organic substrates are oxidized and degraded by serving as electron donors to reduce State I. The catalytic process was selective toward degradation of various aromatic compounds with different substituents, probably depending on the oxidation state of State I and the ionization potential (IP) of the organics; that is, only those organics with an IP value lower than ca. 9.0 eV can be oxidized in the CPPy-F-8/PMS system.

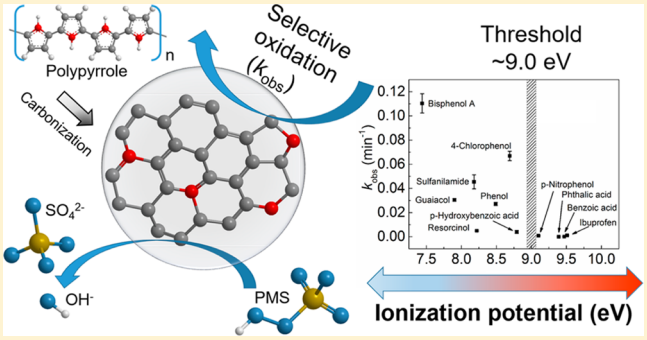

INTRODUCTION

Persulfate (peroxydisulfate (PDS) or peroxymonosulfate (HSO_5^-, PMS)) is playing an emerging role in advanced oxidation processes because it can be activated to readily produce highly reactive sulfate radicals ($SO_4^{\bullet-}$, oxidation potential is 2.5−3.1 V versus normal hydrogen electrode) over a wide range of solution pHs (2−8).[1] Similar to Fenton's reaction, coupling persulfate and transition metal ions (Co^{2+}, Mn^{2+}, Fe^{2+}, etc.) is an effective strategy by which to produce $SO_4^{\bullet-}$, and PMS has attracted increasing attention due to its high efficiency to degrade organic pollutants.[2,3] Considering the potential toxicity and secondary pollution of dissolved metal ions, there is growing interest to develop heterogeneous metal-containing catalysts to activate PMS, including metal oxides (Co_3O_4, Mn_2O_3, CuO, etc.), metal organic frameworks (MOFs), and a myriad of supported metallic catalysts.[4−10] However, despite their high efficiency for activating PMS, the leaching of toxic metal ions remains a significant concern. Recently, metal-free catalysts for PMS activation, such as carbon-,[11] boron-,[12] and sulfur-based[13] materials, are becoming an important research topic. Among these metal-free catalysts, nitrogen-doped carbonaceous materials, such as N-doped reduced graphene oxide (N-rGO), carbon nanotubes (N-CNTs), and nanodiamonds, have been investigated.[14−16] N-rGO was reported to activate PMS and degrade phenol as efficiently as Co_3O_4 or α-MnO_2.[17] In addition, sulfur and boron can also be introduced into nitrogen-doped carbonaceous materials to further improve catalytic performance due to the modulation of chemical properties and creation of new active sites.[17−19] Generally, these N-doped materials are prepared by surface modification and thermal treatment with external

Received: June 12, 2017
Revised: August 22, 2017
Accepted: August 31, 2017
Published: August 31, 2017

DOI: 10.1021/acs.est.7b03014
Environ. Sci. Technol. 2017, 51, 11288−11296

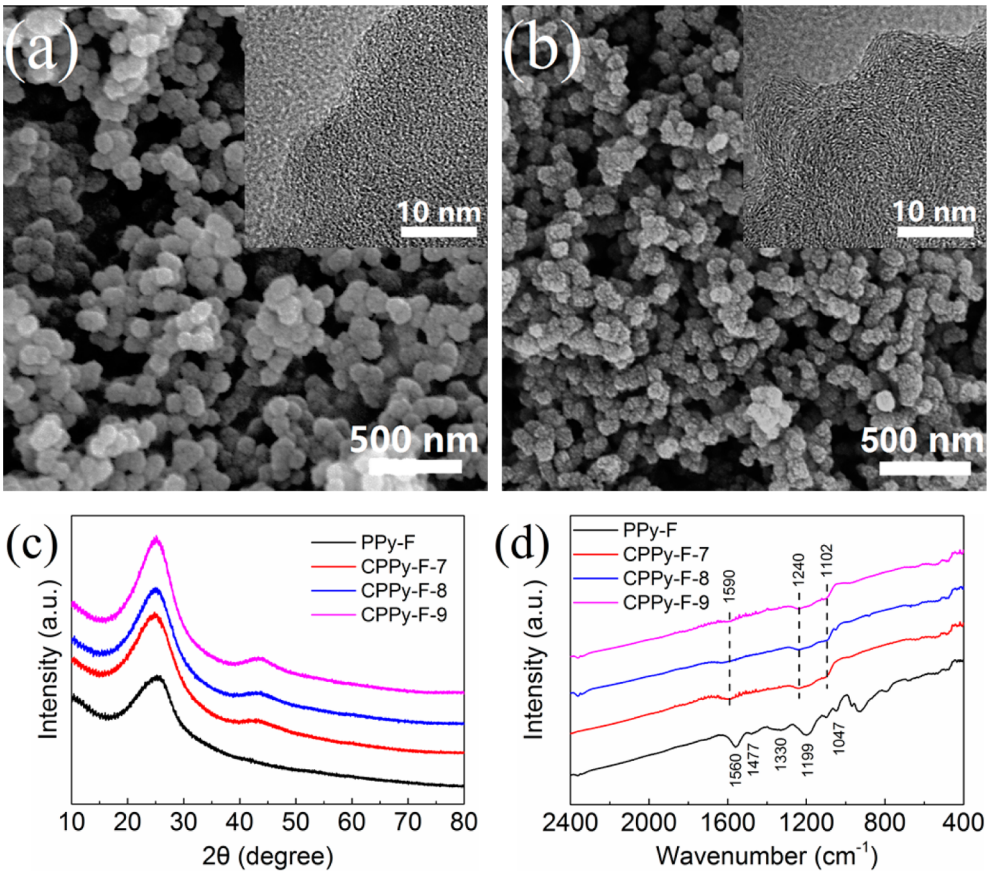

Figure 1. SEM images (insets: HRTEM images) of (a) PPy-F and (b) CPPy-F-8. (c) XRD patterns and (d) FT-IR spectra of PPy-F and CPPy-F-*T*.

nitrogen sources, such as ammonium nitrate, urea, and melamine, increasing synthesis complexity.

The activation of PMS usually involves the generation of free radicals such as $SO_4^{\bullet-}$ and $^{\bullet}OH$. However, a nonradical PMS activation pathway, in which organics can be degraded in the absence of radicals, has also been reported recently.[20,21] Specifically, benzoquinone was reported to activate PMS to produce singlet oxygen ($^1O_2$) rather than radicals for the degradation of sulfamethoxazole.[22] This process widens the application of PMS in decontamination without the worry about radical scavengers in a complex environment. In heterogeneous catalytic systems using carbocatalysts, the mechanisms (radical versus nonradical) of PMS activation remains controversial.[23,24] Wang et al. found that $SO_4^{\bullet-}$ and $^{\bullet}OH$ were produced in an N-doped graphene (NG)/PMS system and played a vital role in phenol degradation.[25] Furthermore, Duan et al. claimed that $SO_4^{\bullet-}$ and $^{\bullet}OH$ were responsible for phenol degradation using nitrogen-modified nanodiamonds as catalysts for PMS activation based on electron paramagnetic resonance (EPR) measurements, and theoretical calculations showed that the prolonged O−O bond of adsorbed PMS on the catalyst surface favored the generation of radicals.[16] Nevertheless, recently, Liang et al. identified $^1O_2$ after the activation of PMS by NG and proposed it as the main nonradical species for organic degradation.[26] Lee et al. proposed that a nonradical mechanism was involved in phenol oxidation, in which persulfates and phenol were likely to form a charge-transfer complex on the surface of graphited nanodiamond.[27] More commonly, nonradical activation was found to coexist with radical pathways in PMS activation by carbonaceous materials.[27−29] Generally speaking, the mechanism of nonradical activation pathway of PMS remains blurred and largely unexplored.

Polypyrrole (PPy) is a nitrogen-containing conducting polymer. Due to its high electrical conductivity, electrochemical activity and chemical stability, PPy has become a promising material for supercapacitors.[30,31] Currently, PPy-derived carbon materials are widely used as lithium-ion battery anodes,[32] capacitors,[33] and electrocatalysts for oxygen reduction reactions.[34] The introduction of nitrogen into carbon matrix can be directly achieved by the pyrolysis of PPy without addition of any nitrogen-containing precursor.[35] The in situ generation of nitrogen dopants in PPy-derived carbon would result in relatively high contents of active sites and lead to enhanced performance in catalytic applications.

Herein, N-doped carbonaceous nanosphere catalysts were developed by carbonization of PPy, a source of both carbon and nitrogen, and their catalytic performance of PMS activation for organics removal was evaluated for the first time. The catalysts exhibited excellent catalytic activity over a wide range of solution pH values and displayed selective degradation for different aromatic compounds via the activation of PMS. A two-step catalytic mechanism is proposed in which the catalyst produces a metastable state through the transfer of electrons to PMS and subsequently reacts selectively with organics with different ionization potentials.

■ EXPERIMENTAL SECTION

Synthesis of Catalysts. The catalysts were made by carbonization of precursor PPy nanospheres (PPy-F), which

DOI: 10.1021/acs.est.7b03014
Environ. Sci. Technol. 2017, 51, 11288−11296

were synthesized through a scalable chemical oxidative polymerization method (a detailed synthesis procedure can be found in Text S1). Briefly, PPy-F was heated at 350 °C for 2 h and further calcined at different temperatures for 2 h in a tubular furnace under an argon atmosphere (Ar flow rate was 100 mL/min, and ramping rate was 2 °C/min). Next, the samples were rinsed with deionized water and ethanol several times and dried. The final products are referred as CPPy-F-*T*, in which *T* represents the calcination temperature (*T* = 7, 8 and 9, corresponding to 700, 800, and 900 °C, respectively). Characterization of the as-prepared samples is described in Text S2.

Activity Evaluation. Phenol was selected to evaluate the catalytic activity of the catalysts, and Oxone ($2KHSO_5 \cdot KHSO_4 \cdot K_2SO_4$, J&K Scientific Ltd.) was used as the source of PMS. In a typical experiment, the reaction was initiated by addition of 0.1 g of Oxone (0.325 mmol PMS) to phenol solution (100 mL) containing 0.01 g of catalyst. The reaction system was kept in a water bath at 25 °C. At certain intervals, 0.5 mL of sample was withdrawn and filtered into a high-performance liquid chromatography (HPLC) vial containing 0.5 mL of methanol to terminate the catalytic reaction. The concentration of phenol was analyzed by HPLC (LC-2010AHT, Shimadzu). To investigate the mechanism of catalytic reactions, several other organic compounds were also tested (listed in Table S1, with detailed HPLC analytical conditions). EPR measurement was carried out on a Bruker ELEXSYS 580 spectrometer to detect free radicals during the PMS activation using 5,5-dimethyl-1-pyrroline *N*-oxide (DMPO, 98%, Adams Reagent Co., Ltd.) as the spin-trapping agent. The determination of PMS concentration in reaction solution was conducted based on a modified 2,2'-azino-bis(3-ethylbenzothiazoline-6-sulfonic acid) diammonium salt (ABTS) method, as we previously reported.[36]

RESULTS AND DISCUSSION

Characterization of Catalysts. PPy-F features nanosphere morphology with a diameter of ca. 86 nm (Figure 1a). The triblock polymer (P123) was used to enhance the solubility of pyrrole monomers under a mild condition and improve the production of PPy. Sphere-like micelles can spontaneously form in P123 aqueous solution, and pyrrole monomers tend to enter the interior of the micelles and polymerize into nanospheres.[37] CPPy-F samples after carbonization possess similar morphologies to the precursor PPy-F but with coarser surfaces and slightly smaller particle sizes (Figures 1b and S1) because of the thermal break of chemical bonds in the carbonization process. From the inset HRTEM images, fringes can be clearly identified at the margins of the samples after carbonization, which indicates the partial graphitization of amorphous carbon at high temperatures.[38]

The XRD pattern of PPy-F (Figure 1c) only shows a broad band at $2\theta = 25°$, indicating typical nanostructured polymers with a low degree of crystallinity.[39] However, those of CPPy-F-*T* samples exhibit two bands at around 25° and 43.5°, which can be assigned to the (0 0 2) and (1 0 0) planes of carbon, respectively, suggesting the graphitization of the samples.[40] In spite of the slight increase of the intensity of the two typical bands with the rising calcination temperature, the graphitization degree is still at a low level because of the intrinsic hard carbon property of PPy. Figure 1d shows the Fourier transform infrared (FT-IR) spectra of PPy-F and CPPy-F samples. In the spectrum of PPy-F, typical peaks of PPy, such as the in-plane bending vibration of C−H and C−N at 1330 and 1047 cm^{-1},[41] the stretching vibration of C−N−C at 1199 cm^{-1},[42] and the asymmetrical and symmetrical stretching vibrations of C−C at 1560 and 1477 cm^{-1},[43] can be explicitly identified. However, the above-mentioned peaks of PPy almost disappear and some new peaks emerge after carbonization. The peak at 1590 cm^{-1} is attributed to the stretching vibration of C=N and C=C, and the peaks at 1240 and 1102 cm^{-1} are assigned to the stretching vibration of C−N.[44,45] The results indicate that nitrogen is successfully doped into the carbon substrate, while oxygen and hydrogen are mostly removed during calcination.

Raman analyses were carried out to further investigate the structural defects of the carbon substrate of the carbonized products (Figure S2a). The integrated intensity ratio (I_D/I_G) of the D band (1363 cm^{-1}) and the G band (1572 cm^{-1}) is known to reflect the defective degree in carbon lattice and is estimated to be 1.90, 1.93, and 2.05 for CPPy-F-7, CPPy-F-8, and CPPy-F-9, respectively. The I_D/I_G value grows greatly for CPPy-F-9, implying the cleavage of chemical bonds and simultaneous reconstruction of carbon substrate, as well as nitrogen doping, during thermal treatment.[44] In addition, CPPy-F-8 has the highest BET specific surface area (74.9 m^2 g^{-1}) among the samples (Figure S2b and Table S2). The PPy chain would decompose at high temperature, creating more edges and fractures. However, the collapse and sintering of carbonaceous materials may occur when the temperature is too high, which has an adverse effect on pore structures. CPPy-F-*T* samples consist mainly of mesopores with average pore diameter in the range of 3.3−3.6 nm, determined based on the Barrett−Joyner−Halenda model.

The changes in chemical composition of the synthesized materials were studied by XPS analyses. XPS survey spectra (Figure 2a) reveal that PPy-F and its corresponding carbonized

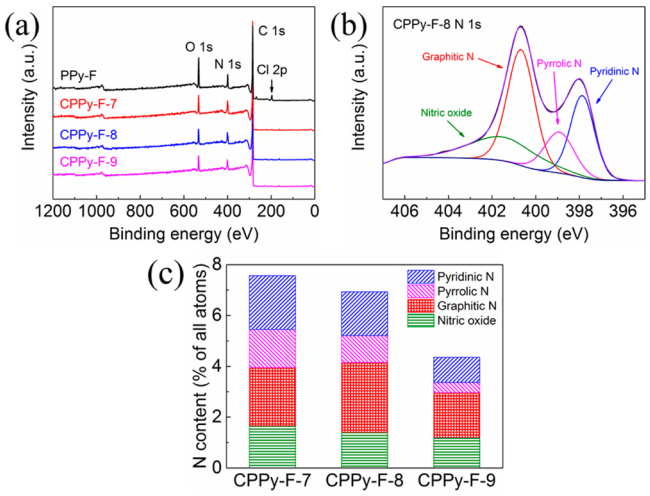

Figure 2. (a) XPS survey of PPy-F and its carbonized products. (b) N 1s spectrum of CPPy-F-8. (c) Contents of four nitrogen species.

products are mainly composed of C, N, and O. In addition, Cl dopant from oxidant used in polymerization can also be found in PPy-F but is almost completely removed after annealing. During the polymerization process, pyrrole monomers form radical cations and react with water molecules through nucleophilic reaction,[46] where oxygen is introduced and the atomic ratio of oxygen reaches 10.4%. However, the oxygen contents drop sharply to 4.9%, 4.1% and 4.1% for CPPy-F-7, CPPy-F-8, and CPPy-F-9, respectively, due to the decom-

DOI: 10.1021/acs.est.7b03014
Environ. Sci. Technol. 2017, 51, 11288−11296

position of oxygen-containing functional groups. Deconvolution of the O 1s spectra (Figure S3) reveals three peaks corresponding to C−O (532.2 eV), O−C=O (533.6 eV), and C=O (530.5 eV),[45] and ketonic groups account for a minor proportion (5.6−7.2%) of all oxygen functional groups.

The nitrogen species in PPy-F are dominated by pyrrolic N−H (399.6 eV), along with −N= (397.8 eV), $-N^+$ (400.4 eV), and $=N^+$ (401.5 eV) (Figure S4a).[47] Nevertheless, as the high-resolution XPS N 1s spectra of CPPy-F-T show (Figures 2b and S4b), significant changes of nitrogen species have taken place after calcination at high temperatures. The ratio of pyrrolic N is reduced, and graphitic N (400.9 eV) and pyridinic N (398.2 eV) form and become dominant.[48,49] The formation of nitric oxide (402.0 eV) can also be discerned.[28] During the annealing, the reconstruction of N and C atoms leads to the transformation from pyrrolic N to a more thermostable structure consisting of graphitic and pyridinic N. Moreover, the C−N bond is more vulnerable during the high-temperature process due to its lower binding energy (305 kJ mol^{-1}) than that of C−C bond (379 kJ mol^{-1}), and the cleavage of C−N bonds derived from rearrangement of carbon framework causes the partial loss of nitrogen (Figure 2c).[50] The N contents decrease from 7.6% (CPPy-F-7) to 4.4% (CPPy-F-9) with the elevation of calcination temperature, and CPPy-F-8 owns the highest graphitic N content (2.7%) among the three carbonized samples (2.3% for CPPy-F-7 and 1.8% for CPPy-F-9).

Catalytic Degradation of Phenol. The catalytic activities of the carbonaceous materials were evaluated by activation of PMS for degradation of phenol in aqueous solution (Figure 3a). PMS did not oxidize phenol without the assistance of catalysts. Similarly, no significant decrease in phenol concentration was observed when CPPy-F-8 is applied alone, indicating poor adsorption of phenol onto the catalyst. Phenol was effectively removed in the presence of both PMS and CPPy-F-8, with a removal efficiency of 97% achieved in 120 min. In contrast, when a nitrogen-free carbonaceous material, CGlu (product of hydrothermal treatment and carbonization of glucose, detailed synthesis procedure given in Text S3), was used as catalyst, phenol removal was negligible. Furthermore, the residual iron species in the carbonized samples are trace (about 0.06 wt % according to graphite furnace atomic absorption spectroscopy measurement) and cannot be detected by XPS (Figure S5). The homogeneous catalytic activation of PMS by Fe^{2+} using the same quantity of iron in the catalysts was also ineffective (Figure S6).

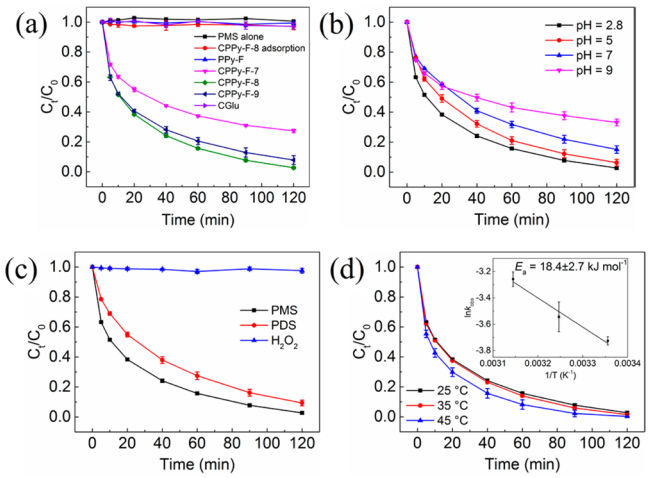

Figure 3. (a) Phenol removal under different conditions. The effects of (b) initial pH, (c) various oxidants, and (d) temperature on phenol degradation using CPPy-F-8 ($[phenol]_0$ = 20 mg L^{-1}, $[oxidant]_0$ = 3.25 mM, [catalyst] = 0.1 g L^{-1}, initial pH = 2.8, T = 25 °C).

PPy-F fails to activate PMS to degrade phenol, while after calcination, the CPPy-F-T samples are all capable of activating PMS (Figure 3a). This suggests that pyrrolic N in a five-membered heterocyclic ring, the main nitrogen species in the precursor PPy-F, is not the active site for catalytic reactions. During calcination, the surface of the carbon substrate is graphitized and nitrogen dopants are formed (Figure 2b), making the N-doped carbon an effective catalyst for PMS activation. Among the carbonized products, CPPy-F-8 exhibits the highest catalytic activity and phenol removal efficiency over 2 h (97%), followed by CPPy-F-9 (92%) and CPPy-F-7 (73%). High calcination temperatures facilitate the formation of crystalline carbon (Figure 1c) and modulate the doped nitrogen species (Figure 2c), enhancing the catalytic performance of PMS activation. When the calcination temperature reaches 900 °C, the abundance of nitrogen dopants and the specific surface area decrease, which adversely effects the catalytic reactivity. However, more defects are created on the carbon substrate, as indicated by the Raman spectra, which favors PMS activation.[51] Therefore, the catalytic activity of CPPy-F-9 only decreases moderately compared with that of CPPy-F-8.

The effect of solution pH was investigated below 9 because PMS would be activated by base under strong basic conditions (pH ≥ 10).[52] Phenol degradation by CPPy-F-8 increases notably from pH 9 to pH 5 but only slightly when pH further decreases to 2.8 (Figure 3b). This is consistent with the change in the ζ-potential of the catalyst (Figure S7). A similar trend was obtained for CPPy-F-9 (Figure S8) and in previous reports on metal-free catalysts.[53] This could be attributed to the protonated nitrogen species, which make the catalyst surface covered with positive charge and facilitate the interaction between the catalyst and negatively charged PMS (HSO_5^-). Overall, the CPPy-F-8/PMS system effectively degrades phenol over a wide range of pH values (2−9), outperforming conventional Fenton or Fenton-like reactions.[54,55] Moreover, the result is also superior to cobalt-mediated PMS activation, in which the formation of critical species $CoOH^+$ is greatly suppressed at relatively acidic conditions.[56] CPPy-F-8 is a versatile catalyst that could also effectively activate PDS to eliminate phenol with 91% efficiency in 120 min (Figure 3c). The slightly inferior performance of PDS is probably due to the symmetric structure of PDS, which is more difficult to activate.[3] However, almost no phenol degradation occurred when H_2O_2 was used as the oxidant. The bond energy of O−O in H_2O_2 (213 kJ mol^{-1}) is much higher than that in persulfate (e.g., PDS (140 kJ mol^{-1})), which may be the reason for the hindered catalytic activation.[57] Elevated temperature plays a trivial role in accelerating phenol degradation in the CPPy-F-8/PMS system (Figure 3d). The apparent activation energy (E_a) is estimated to be 18.4 ± 2.7 kJ mol^{-1} according to the Arrhenius equation, which is lower than those reported modified carbonaceous catalysts such as N-rGO (31.6 kJ mol^{-1}),[44] N-CNT (36.0 kJ mol^{-1}),[28] and NS-CNT (46.3 kJ mol^{-1}).[58] The low E_a value may indicate an efficient reaction process as discussed in the next section.

Catalytic Process Mechanism. Quenching experiments were carried out to explore the mechanism of PMS activation and phenol degradation. Ethanol (EtOH) with α-H is a radical

DOI: 10.1021/acs.est.7b03014
Environ. Sci. Technol. 2017, 51, 11288−11296

scavenger for both •OH (k = (1.2−2.8) × 10^9 M^{-1} s^{-1}) and $SO_4^{\bullet-}$ (k = (1.6−7.7) × 10^7 M^{-1} s^{-1}), while *tert*-butanol (TBA) without α-H is an effective quenching agent for •OH (k = (3.8−7.6) × 10^8 M^{-1} s^{-1}) but not for $SO_4^{\bullet-}$ (k = (4.0−9.1) × 10^5 M^{-1} s^{-1}).[16,36,59−61] Both quenching agents were used in the CPPy-F-8/PMS system (Figure 4a). When the mole ratio

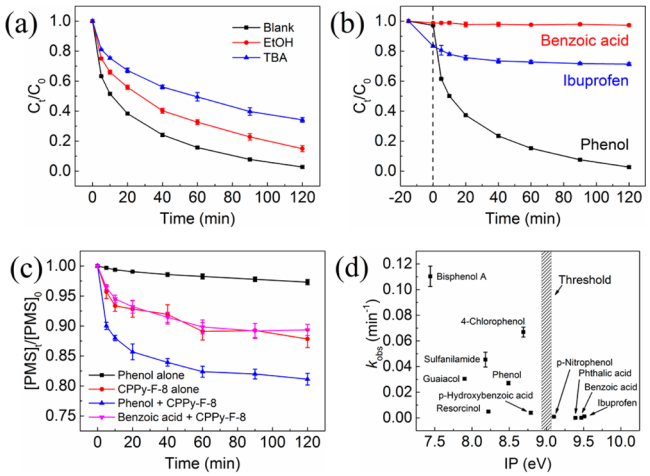

Figure 4. (a) Effect of quenching agents on phenol degradation ($n_{quenching\ agent}/n_{PMS}$ = 1000:1). (b) Adsorption and degradation of different organics using CPPy-F-8. (c) Decomposition of PMS under different conditions. (d) The relationship between ionization potential (IP) and degradation of organics in the CPPy-F-8/PMS system at initial pH 2.8 ($[organics]_0$ = 20 mg L^{-1}, $[PMS]_0$ = 3.25 mM, [CPPy-F-8] = 0.1 g L^{-1}, initial pH = 2.8, T = 25 °C).

of quenching agent to PMS reaches 1000:1, phenol degradation is still not deterred, and 85% and 66% phenol can be eliminated in 120 min in the presence of EtOH and TBA, respectively. Moreover, phenol degradation performance in the presence of EtOH is better than that in the presence of TBA, which is an opposite outcome to that expected from the widely accepted radical pathway of PMS activation by metal ions.[62]

One possible explanation is that free radicals are generated and bonded on the surface of the carbonaceous catalyst during the activation process. TBA is more hydrophobic than EtOH and has a stronger affinity with the catalyst to quench the free radicals, resulting in a poorer phenol degradation performance.[59] To clarify this assumption, ibuprofen, which can be efficiently oxidized by the attack of •OH and $SO_4^{\bullet-}$,[36,63] was selected as a probe in the same catalytic system (Figure 4b). When adsorption equilibrium was achieved (0 min), 17% ibuprofen was removed, indicating a better adsorption ability than that of phenol. However, ibuprofen removal was inappreciable after PMS was added (only 12% removal in 120 min). Furthermore, EPR measurement was also employed to detect the presence of •OH and $SO_4^{\bullet-}$ (Figure S9). In the spectrum of CPPy-F-8/PMS system, the signals of DMPO−OH and DMPO−SO_4 were barely identifiable. A 1:1:1 triplet was detected, which could be ascribed to an oxidation product of DMPO.[64] These results show that PMS decomposition to free radicals mediated by the electron-rich groups in the catalyst (such as ketonic groups) and sp^2 hybridized carbon framework plays a minor role; PMS activation and organic degradation in the CPPy-F-8/PMS system are mainly induced through a nonradical pathway.[51,53,65] In addition, phenol degradation is only slightly reduced in the presence of furfuryl alcohol (Figure S10), a scavenger of singlet oxygen, suggesting the minor contribution of $^1O_2$ in organic degradation.

Figure 4c depicts the decomposition of PMS under different conditions. PMS decomposition is negligible (less than 3% in 120 min) in the mixture solution of phenol and PMS, while quick consumption of PMS (19% in 120 min) occurs with the addition of CPPy-F-8, which corroborates the insignificant interaction between phenol and PMS and the key role of the catalyst. Furthermore, PMS decomposes on CPPy-F-8 by 12% even without phenol, suggesting an interaction between PMS and CPPy-F-8. The sp^2-hybridized graphitic N possesses lone pair electrons, forming delocalized conjugated π systems with sp^2-hybridized carbon frameworks.[66] Moreover, the higher electronegativity enables nitrogen to abstract electrons from adjacent carbon atoms.[67] Accordingly, graphitic N has higher electron cloud density and can serve as active sites to activate and break O−O bond in PMS through electron transfer, resulting in the decomposition of PMS. After being "oxidized" by PMS, the framework of the catalyst carries positive charges and forms a metastable oxidation state (State I) and finally generate more surface oxygen-containing groups (State II) in the absence of organics, which is corroborated by XPS measurement (Figure S11). Simultaneously, the metastable state (State I) of the active sites can react with organics and revert to CPPy-F-8 (Scheme 1). The plausible two-step

Scheme 1. Catalytic Mechanism of CPPy-F-*T*/PMS System

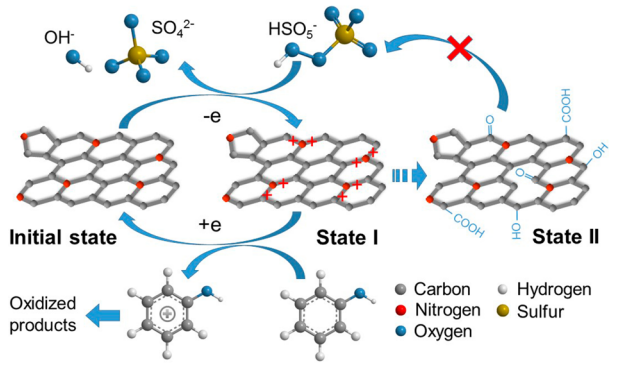

catalytic mechanism of the CPPy-F-8/PMS system is similar to that of heme peroxidases, in which heme-containing enzymes use H_2O_2 as the electron acceptor to catalyze a number of oxidative reactions.[68]

Figure S12 clearly reveals that State II, formed upon interaction between the catalyst and PMS in the absence of organics, is a deactivation state, with only 22% phenol degradation efficiency in 120 min. The spent CPPy-F-8 also displayed a much-poorer phenol degradation performance (39%) than the fresh catalyst (Figure S13). The deactivation accompanying with phenol degradation indicates a competition between the reactions for organic degradation and the formation of State II. The oxygen content of spent CPPy-F-8 increases sharply from 4.1% (fresh CPPy-F-8) to 11.7% according to XPS survey (Figure S14). After a thermal treatment to remove oxygen-containing groups (Figure S14), the catalytic activity of the spent CPPy-F-8 (used twice) could be fully recovered (Figure S13). These results indicate that the catalyst in State II with excessive oxygen species, featuring a disturbed sp^2 carbon framework, relatively high oxidation state, and disordered electron configuration, is unfavorable for electron transfer from the catalyst to PMS.[16,51,69]

DOI: 10.1021/acs.est.7b03014
Environ. Sci. Technol. 2017, 51, 11288−11296

In contrast to phenol, benzoic acid has no influence on the decomposition of PMS (Figure 4c) and cannot be degraded in the CPPy-F-8/PMS system (Figure 4b), indicating that a substrate dependency is involved in the catalytic reaction. Various aromatic compounds were further tested in the CPPy-F-8/PMS system at pH 2.8 and 7 (Figure S15), and results show a notable selectivity of the catalytic system in degradation of aromatic organics. All phenolic compounds except *p*-nitrophenol can be removed to a large degree, while benzoic acid and its derivatives display negligible degradation except for *p*-hydroxybenzoic acid, which shows low degradation rates (k_{obs} of 0.004 and 0.002 min^{-1} at pH 2.8 and 7, respectively). This selectivity was also observed in a mixture solution of phenol and benzoic acid (Figure S16). This selective oxidation can be attributed to more than just their different affinities toward catalyst surface because no obvious correlation between adsorption onto CPPy-F-8 (q_e) and degradation (k_{obs}) in the CPPy-F-8/PMS system is observed (Figure S17).[70,71]

Generally, physicochemical properties and substituents of organics may strongly affect their reactivity in oxidation processes.[72−75] Among various molecular descriptors, ionization potential (IP) was found closely related to the reaction rates in several oxidation systems.[73,76,77] Moreover, electron-donating groups, such as hydroxyl and amido, can lower the IP of the organics, while electron-withdrawing groups, such as carboxyl and nitryl, have an opposite effect.[78] A relationship between IP values and degradation rate constants of aromatic compounds in the CPPy-F-8/PMS system is plotted in Figure 4d (pH 2.8) and Figure S18 (pH 7). There is a probable IP threshold at ca. 9.0 eV, corresponding to the oxidation ability of State I to react with organics. Those organic substrates with higher IP values (Table S3) than the threshold cannot serve as electron donors and be oxidized by State I (Scheme 1). According to the distinct HPLC patterns during the phenol degradation in Co^{2+}/PMS (generally regarded as a radical-induced oxidation process)[79] and CPPy-F-8/PMS systems (Figure S19), oxidized phenol in the primary step may subsequently turn into complex, insoluble intermediates such as phenoxyphenol or dihydroxybiphenyl, with unfavorable formation of *p*-benzoquinone, a typical intermediate in phenol degradation by the attack of radicals. The poor adsorption and negligible degradation of *p*-benzoquinone in the CPPy-F-8/PMS system was proven (Figure S20), and this can be understood by its high IP value (9.96 eV).

Environmental Implications. This study demonstrated PMS activation by a PPy-derived carbocatalyst for degradation of organic contaminants in water. The catalytic reactions take place through a nonradical pathway and display strong selectivity in the removal of aromatic compounds, which depends strongly on the IP values of the organics. Although nonradical reaction possesses a mild oxidation potential, the selectivity of this reaction enables the transformation of target phenolic compounds with low IP values and avoids the competitive reactions with coexisting constituents in a complex environment. Moreover, our study developed a facile, low-cost and scalable approach to synthesize this metal-free catalyst by carbonization of PPy nanospheres. The method could be generalized to other nitrogen-containing polymer or biomass to generate carbocatalysts with higher N dopant contents than those using external nitrogen sources. This facilitates the realization of the multiple advantages of carbocatalysts, e.g., no leachate of metal ions, low cost, and high selectivity, without suffering from the limitations of low N content and low reactivation efficiency and provides an improved family of catalysts for remediation of groundwater, soil and sediment.

The nonradical reaction in PMS activation by CPPy-F is proposed as a two-step process. According to this mechanism, deactivation occurs inherently, but the stability could be improved under fast organics conversion with reduced persulfate dosage (Figure S21), which makes the carbocatalyst suitable for removal of trace organic pollutants. In addition, we can expect easier post-treatment (such as UV irradiation or chemical methods) to recover the carbocatalysts and make it feasible for practical applications. Because the investigations on the catalytic mechanism and selective degradation are still at the primary stage, further insights are needed to discern the structure−activity relationship of the organics as well as their primary degradation pathways.

■ ASSOCIATED CONTENT

Supporting Information

The Supporting Information is available free of charge on the ACS Publications website at DOI: 10.1021/acs.est.7b03014.

Additional details on synthesis procedure and characterization of materials, HPLC analytic conditions and ionization potentials, additional characterization results and catalytic experiments, EPR spectra, reusability of the catalysts, relationships between adsorption or ionization potential and degradation of various aromatic compounds, and HPLC patterns. (PDF)

■ AUTHOR INFORMATION

Corresponding Author

*Phone: 86-21-54747354; fax: 86-21-54740825; e-mail: long_mc@sjtu.edu.cn.

ORCID

Chunyang Yu: 0000-0003-1175-8362
Qilin Li: 0000-0001-5756-3873
Baoxue Zhou: 0000-0001-6957-190X
Pedro J. J. Alvarez: 0000-0002-6725-7199
Mingce Long: 0000-0002-5168-8330

Notes

The authors declare no competing financial interest.

■ ACKNOWLEDGMENTS

Financial support from the Natural Science Foundation of China (no. 21377084), the Special Fund for Agro-Scientific Research in the Public Interest (no. 201503107), and the Shanghai Municipal International Cooperation Foundation (no. 15230724600) is gratefully acknowledged. Partial support was provided by the NSF ERC on Nanotechnology-Enabled Water Treatment (no. EEC-1449500). We gratefully acknowledge the support in XPS and ζ-potential measurements and valuable suggestions by Mr. Ligang Zhou of the Instrumental Analysis Center and Ms. Xiaojuan Yu of School of Environmental Science and Engineering of Shanghai Jiao Tong University.

■ REFERENCES

(1) Hu, P.; Long, M. Cobalt-catalyzed sulfate radical-based advanced oxidation: A review on heterogeneous catalysts and applications. *Appl. Catal., B* **2016**, *181*, 103−117.

(2) Anipsitakis, G. P.; Dionysiou, D. D. Degradation of organic contaminants in water with sulfate radicals generated by the

DOI: 10.1021/acs.est.7b03014
Environ. Sci. Technol. 2017, 51, 11288−11296

conjunction of peroxymonosulfate with cobalt. *Environ. Sci. Technol.* **2003**, *37* (20), 4790−4797.
(3) Chen, X.; Wang, W.; Xiao, H.; Hong, C.; Zhu, F.; Yao, Y.; Xue, Z. Accelerated TiO_2 photocatalytic degradation of Acid Orange 7 under visible light mediated by peroxymonosulfate. *Chem. Eng. J.* **2012**, *193−194* (12), 290−295.
(4) Anipsitakis, G. P.; Stathatos, E.; Dionysiou, D. D. Heterogeneous activation of oxone using Co_3O_4. *J. Phys. Chem. B* **2005**, *109* (27), 13052−13055.
(5) Saputra, E.; Muhammad, S.; Sun, H.; Ang, H.-M.; Tadé, M. O.; Wang, S. Manganese oxides at different oxidation states for heterogeneous activation of peroxymonosulfate for phenol degradation in aqueous solutions. *Appl. Catal., B* **2013**, *142−143*, 729−735.
(6) Ji, F.; Li, C.; Deng, L. Performance of CuO/Oxone system: Heterogeneous catalytic oxidation of phenol at ambient conditions. *Chem. Eng. J.* **2011**, *178* (1), 239−243.
(7) Andrew Lin, K.-Y.; Chang, H.-A. Zeolitic Imidazole Framework-67 (ZIF-67) as a heterogeneous catalyst to activate peroxymonosulfate for degradation of Rhodamine B in water. *J. Taiwan Inst. Chem. Eng.* **2015**, *53*, 40−45.
(8) Andrew Lin, K.-Y.; Hsu, F.-K.; Lee, W.-D. Magnetic cobalt−graphene nanocomposite derived from self-assembly of MOFs with graphene oxide as an activator for peroxymonosulfate. *J. Mater. Chem. A* **2015**, *3* (18), 9480−9490.
(9) Huang, Z.; Bao, H.; Yao, Y.; Lu, W.; Chen, W. Novel green activation processes and mechanism of peroxymonosulfate based on supported cobalt phthalocyanine catalyst. *Appl. Catal., B* **2014**, *154−155*, 36−43.
(10) Stoyanova, M.; Slavova, I.; Christoskova, S.; Ivanova, V. Catalytic performance of supported nanosized cobalt and iron−cobalt mixed oxides on MgO in oxidative degradation of Acid Orange 7 azo dye with peroxymonosulfate. *Appl. Catal., A* **2014**, *476* (6), 121−132.
(11) Sun, H.; Liu, S.; Zhou, G.; Ang, H. M.; Tade, M. O.; Wang, S. Reduced graphene oxide for catalytic oxidation of aqueous organic pollutants. *ACS Appl. Mater. Interfaces* **2012**, *4* (10), 5466−5471.
(12) Shao, P.; Duan, X.; Xu, J.; Tian, J.; Shi, W.; Gao, S.; Xu, M.; Cui, F.; Wang, S. Heterogeneous activation of peroxymonosulfate by amorphous boron for degradation of bisphenol S. *J. Hazard. Mater.* **2017**, *322*, 532−539.
(13) Andrew Lin, K.-Y.; Zhang, Z.-Y. α-Sulfur as a metal-free catalyst to activate peroxymonosulfate under visible light irradiation for decolorization. *RSC Adv.* **2016**, *6* (18), 15027−15034.
(14) Peng, W.; Liu, S.; Sun, H.; Yao, Y.; Zhi, L.; Wang, S. Synthesis of porous reduced graphene oxide as metal-free carbon for adsorption and catalytic oxidation of organics in water. *J. Mater. Chem. A* **2013**, *1* (19), 5854−5859.
(15) Sun, H.; Kwan, C.; Suvorova, A.; Ang, H. M.; Tadé, M. O.; Wang, S. Catalytic oxidation of organic pollutants on pristine and surface nitrogen-modified carbon nanotubes with sulfate radicals. *Appl. Catal., B* **2014**, *154−155* (5), 134−141.
(16) Duan, X.; Ao, Z.; Li, D.; Sun, H.; Zhou, L.; Suvorova, A.; Saunders, M.; Wang, G.; Wang, S. Surface-tailored nanodiamonds as excellent metal-free catalysts for organic oxidation. *Carbon* **2016**, *103*, 404−411.
(17) Sun, H.; Wang, Y.; Liu, S.; Ge, L.; Wang, L.; Zhu, Z.; Wang, S. Facile synthesis of nitrogen doped reduced graphene oxide as a superior metal-free catalyst for oxidation. *Chem. Commun.* **2013**, *49* (85), 9914−9916.
(18) Duan, X. G.; O'Donnell, K.; Sun, H. Q.; Wang, Y. X.; Wang, S. B. Sulfur and nitrogen co-doped graphene for metal-free catalytic oxidation reactions. *Small* **2015**, *11* (25), 3036−3044.
(19) Tian, W.; Zhang, H.; Duan, X.; Sun, H.; Tade, M. O.; Ang, H. M.; Wang, S. Nitrogen- and sulfur-codoped hierarchically porous carbon for adsorptive and oxidative removal of pharmaceutical contaminants. *ACS Appl. Mater. Interfaces* **2016**, *8* (11), 7184−7193.
(20) Duan, X. G.; Sun, H. Q.; Wang, Y. X.; Kang, J.; Wang, S. B. N-doping-induced nonradical reaction on single-walled carbon nanotubes for catalytic phenol oxidation. *ACS Catal.* **2015**, *5* (2), 553−559.
(21) Duan, X. G.; Ao, Z. M.; Sun, H. Q.; Zhou, L.; Wang, G. X.; Wang, S. B. Insights into N-doping in single-walled carbon nanotubes for enhanced activation of superoxides: a mechanistic study. *Chem. Commun.* **2015**, *51* (83), 15249−15252.
(22) Zhou, Y.; Jiang, J.; Gao, Y.; Ma, J.; Pang, S. Y.; Li, J.; Lu, X. T.; Yuan, L. P. Activation of peroxymonosulfate by benzoquinone: A novel nonradical oxidation process. *Environ. Sci. Technol.* **2015**, *49* (21), 12941−12950.
(23) Duan, X.; Sun, H.; Wang, S. Comment on "Activation of Persulfate by Graphitized Nanodiamonds for Removal of Organic Compounds". *Environ. Sci. Technol.* **2017**, *51* (9), 5351−5352.
(24) Lee, H.; Lee, C.; Kim, J. H. Response to comment on "Activation of Persulfate by Graphitized Nanodiamonds for Removal of Organic Compounds". *Environ. Sci. Technol.* **2017**, *51* (9), 5353−5354.
(25) Wang, C.; Kang, J.; Sun, H. Q.; Ang, H. M.; Tade, M. O.; Wang, S. B. One-pot synthesis of N-doped graphene for metal-free advanced oxidation processes. *Carbon* **2016**, *102*, 279−287.
(26) Liang, P.; Zhang, C.; Duan, X.; Sun, H.; Liu, S.; Tade, M. O.; Wang, S. An insight into metal organic framework derived N-doped graphene for the oxidative degradation of persistent contaminants: formation mechanism and generation of singlet oxygen from peroxymonosulfate. *Environ. Sci.: Nano* **2017**, *4* (2), 315−324.
(27) Lee, H.; Kim, H. I.; Weon, S.; Choi, W.; Hwang, Y. S.; Seo, J.; Lee, C.; Kim, J. H. Activation of persulfates by graphitized nanodiamonds for removal of organic compounds. *Environ. Sci. Technol.* **2016**, *50* (18), 10134−10142.
(28) Duan, X.; Sun, H.; Wang, Y.; Kang, J.; Wang, S. N-doping-induced nonradical reaction on single-walled carbon nanotubes for catalytic phenol oxidation. *ACS Catal.* **2015**, *5* (2), 553−559.
(29) Wei, M.; Gao, L.; Li, J.; Fang, J.; Cai, W.; Li, X.; Xu, A. Activation of peroxymonosulfate by graphitic carbon nitride loaded on activated carbon for organic pollutants degradation. *J. Hazard. Mater.* **2016**, *316*, 60−68.
(30) Cao, J.; Wang, Y.; Chen, J.; Li, X.; Walsh, F. C.; Ouyang, J.-H.; Jia, D.; Zhou, Y. Three-dimensional graphene oxide/polypyrrole composite electrodes fabricated by one-step electrodeposition for high performance supercapacitors. *J. Mater. Chem. A* **2015**, *3* (27), 14445−14457.
(31) Tao, J.; Ma, W.; Liu, N.; Ren, X.; Shi, Y.; Su, J.; Gao, Y. High-performance solid-state supercapacitors fabricated by pencil drawing and polypyrrole depositing on paper substrate. *Nano-Micro Lett.* **2015**, *7* (3), 276−281.
(32) Jin, B.; Gao, F.; Zhu, Y. F.; Lang, X. Y.; Han, G. F.; Gao, W.; Wen, Z.; Zhao, M.; Li, J. C.; Jiang, Q. Facile Synthesis of Non-Graphitizable Polypyrrole-Derived Carbon/Carbon Nanotubes for Lithium-ion Batteries. *Sci. Rep.* **2016**, *6*, 19317.
(33) Shrestha, S.; Morse, N.; Mustain, W. E. Effect of surface chemistry on the double layer capacitance of polypyrrole-derived ordered mesoporous carbon. *RSC Adv.* **2014**, *4* (87), 47039−47046.
(34) Meng, Y.; Voiry, D.; Goswami, A.; Zou, X.; Huang, X.; Chhowalla, M.; Liu, Z.; Asefa, T. N-, O-, and S-tridoped nanoporous carbons as selective catalysts for oxygen reduction and alcohol oxidation reactions. *J. Am. Chem. Soc.* **2014**, *136* (39), 13554−13557.
(35) Zhang, F.-F.; Wang, C.-L.; Huang, G.; Yin, D.-M.; Wang, L.-M. Enhanced electrochemical performance by a three-dimensional interconnected porous nitrogen-doped graphene/carbonized polypyrrole composite for lithium−sulfur batteries. *RSC Adv.* **2016**, *6* (31), 26264−26270.
(36) Hu, P.; Long, M.; Bai, X.; Wang, C.; Cai, C.; Fu, J.; Zhou, B.; Zhou, Y. Monolithic cobalt-doped carbon aerogel for efficient catalytic activation of peroxymonosulfate in water. *J. Hazard. Mater.* **2017**, *332*, 195−204.
(37) Zhang, X.; Zhang, J.; Song, W.; Liu, Z. Controllable synthesis of conducting polypyrrole nanostructures. *J. Phys. Chem. B* **2006**, *110* (3), 1158−1165.
(38) Pol, V. G.; Shrestha, L. K.; Ariga, K. Tunable, functional carbon spheres derived from rapid synthesis of resorcinol-formaldehyde resins. *ACS Appl. Mater. Interfaces* **2014**, *6* (13), 10649−10655.

DOI: 10.1021/acs.est.7b03014
Environ. Sci. Technol. 2017, 51, 11288−11296

(39) Sanches, E. A.; Alves, S. F.; Soares, J. C.; da Silva, A. M.; da Silva, C. G.; de Souza, S. M.; da Frota, H. O. Nanostructured Polypyrrole Powder: A Structural and Morphological Characterization. *J. Nanomater.* **2015**, *2015*, 1−8.
(40) Oh, W. K.; Yoon, H.; Jang, J. Size control of magnetic carbon nanoparticles for drug delivery. *Biomaterials* **2010**, *31* (6), 1342−1348.
(41) Blinova, N. V.; Stejskal, J.; Trchova, M.; Prokeš, J.; Omastová, M. Polyaniline and polypyrrole: A comparative study of the preparation. *Eur. Polym. J.* **2007**, *43* (6), 2331−2341.
(42) Sahoo, N. G.; Jung, Y. C.; So, H. H.; Cho, J. W. Polypyrrole coated carbon nanotubes: Synthesis, characterization, and enhanced electrical properties. *Synth. Met.* **2007**, *157* (8−9), 374−379.
(43) Wu, T.-M.; Chang, H.-L.; Lin, Y.-W. Synthesis and characterization of conductive polypyrrole/multi-walled carbon nanotubes composites with improved solubility and conductivity. *Compos. Sci. Technol.* **2009**, *69* (5), 639−644.
(44) Indrawirawan, S.; Sun, H. Q.; Duan, X. G.; Wang, S. B. Low temperature combustion synthesis of nitrogen-doped graphene for metal-free catalytic oxidation. *J. Mater. Chem. A* **2015**, *3* (7), 3432−3440.
(45) Yang, S.; Li, L.; Xiao, T.; Zheng, D.; Zhang, Y. Role of surface chemistry in modified ACF (activated carbon fiber)-catalyzed peroxymonosulfate oxidation. *Appl. Surf. Sci.* **2016**, *383*, 142−150.
(46) Liu, J.; Wan, M. Synthesis, characterization and electrical properties of microtubules of polypyrrole synthesized by a template-free method. *J. Mater. Chem.* **2001**, *11* (2), 404−407.
(47) Menon, V. P.; Lei, J.; Martin, C. R. Investigation of molecular and supermolecular structure in template-synthesized polypyrrole tubules and fibrils. *Chem. Mater.* **1996**, *8* (9), 2382−2390.
(48) Sun, G. L.; Ma, L. Y.; Ran, J. B.; Li, B.; Shen, X. Y.; Tong, H. Templated synthesis and activation of highly nitrogen-doped worm-like carbon composites based on melamine-urea-formaldehyde resins for high performance supercapacitors. *Electrochim. Acta* **2016**, *194*, 168−178.
(49) Chen, Y.; Li, J.; Yue, G.; Luo, X. Novel Ag@nitrogen-doped porous carbon composite with high electrochemical performance as anode materials for lithium-ion batteries. *Nano-Micro Lett.* **2017**, *9* (3), 32.
(50) Wang, L.; Gao, Z. Y.; Chang, J. L.; Liu, X.; Wu, D. P.; Xu, F.; Guo, Y. M.; Jiang, K. Nitrogen-doped porous carbons as electrode materials for high-performance supercapacitor and dye-sensitized solar cell. *ACS Appl. Mater. Interfaces* **2015**, *7* (36), 20234−20244.
(51) Duan, X. G.; Sun, H. Q.; Ao, Z. M.; Zhou, L.; Wang, G. X.; Wang, S. B. Unveiling the active sites of graphene-catalyzed peroxymonosulfate activation. *Carbon* **2016**, *107*, 371−378.
(52) Chen, J.; Zhang, L.; Huang, T.; Li, W.; Wang, Y.; Wang, Z. Decolorization of azo dye by peroxymonosulfate activated by carbon nanotube: Radical versus non-radical mechanism. *J. Hazard. Mater.* **2016**, *320*, 571−580.
(53) Li, D.; Duan, X.; Sun, H.; Kang, J.; Zhang, H.; Tade, M. O.; Wang, S. Facile synthesis of nitrogen-doped graphene via low-temperature pyrolysis: The effects of precursors and annealing ambience on metal-free catalytic oxidation. *Carbon* **2017**, *115*, 649−658.
(54) Ramirez, J. H.; Costa, C. A.; Madeira, L. M.; Mata, G.; Vicente, M. A.; Rojas-Cervantes, M. L.; López-Peinado, A. J.; Martín-Aranda, R. M. Fenton-like oxidation of Orange II solutions using heterogeneous catalysts based on saponite clay. *Appl. Catal., B* **2007**, *71* (1−2), 44−56.
(55) Kang, Y. W.; Hwang, K.-Y. Effects of reaction conditions on the oxidation efficiency in the Fenton process. *Water Res.* **2000**, *34* (10), 2786−2790.
(56) Zhu, Y.; Chen, S.; Quan, X.; Zhang, Y. Cobalt implanted TiO_2 nanocatalyst for heterogeneous activation of peroxymonosulfate. *RSC Adv.* **2013**, *3* (2), 520−525.
(57) Yang, S.; Wang, P.; Yang, X.; Shan, L.; Zhang, W.; Shao, X.; Niu, R. Degradation efficiencies of azo dye Acid Orange 7 by the interaction of heat, UV and anions with common oxidants: Persulfate, peroxymonosulfate and hydrogen peroxide. *J. Hazard. Mater.* **2010**, *179* (1−3), 552−558.
(58) Liu, H.; Sun, P.; Feng, M. B.; Liu, H. X.; Yang, S. G.; Wang, L. S.; Wang, Z. Y. Nitrogen and sulfur co-doped CNT-COOH as an efficient metal-free catalyst for the degradation of UV filter BP-4 based on sulfate radicals. *Appl. Catal., B* **2016**, *187*, 1−10.
(59) Yao, Y.; Chen, H.; Lian, C.; Wei, F.; Zhang, D.; Wu, G.; Chen, B.; Wang, S. Ni nanocrystals encapsulated in nitrogen-doped carbon nanotubes as Fenton-like catalysts for organic pollutant removal. *J. Hazard. Mater.* **2016**, *314*, 129−139.
(60) Neta, P.; Huie, R. E.; Ross, A. B. Rate constants for reactions of inorganic radicals in aqueous solution. *J. Phys. Chem. Ref. Data* **1988**, *17* (3), 1027−1284.
(61) Buxton, G. V.; Greenstock, C. L.; Helman, W. P.; Ross, A. B. Critical Review of rate constants for reactions of hydrated electrons, hydrogen atoms and hydroxyl radicals ($\cdot OH/\cdot O^-$) in aqueous solution. *J. Phys. Chem. Ref. Data* **1988**, *17* (2), 513−886.
(62) Liu, J.; Zhao, Z.; Shao, P.; Cui, F. Activation of peroxymonosulfate with magnetic Fe_3O_4−MnO_2 core−shell nanocomposites for 4-chlorophenol degradation. *Chem. Eng. J.* **2015**, *262*, 854−861.
(63) Gong, H.; Chu, W.; Lam, S. H.; Lin, A. Y.-C. Ibuprofen degradation and toxicity evolution during Fe^{2+}/Oxone/UV process. *Chemosphere* **2017**, *167*, 415−421.
(64) Buettner, G. R. Spin trapping: ESR parameters of spin adducts. *Free Radical Biol. Med.* **1987**, *3* (4), 259−303.
(65) Duan, X. G.; Ao, Z. M.; Zhou, L.; Sun, H. Q.; Wang, G. X.; Wang, S. B. Occurrence of radical and nonradical pathways from carbocatalysts for aqueous and nonaqueous catalytic oxidation. *Appl. Catal., B* **2016**, *188*, 98−105.
(66) He, G.; Qiao, M.; Li, W.; Lu, Y.; Zhao, T.; Zou, R.; Li, B.; Darr, J. A.; Hu, J.; Titirici, M. M.; Parkin, I. P. S N-Co-doped graphene-nickel cobalt sulfide aerogel: Improved energy storage and electrocatalytic performance. *Adv. Sci.* **2017**, *4* (1), 1600214.
(67) Wang, H.; Zhang, C.; Liu, Z.; Wang, L.; Han, P.; Xu, H.; Zhang, K.; Dong, S.; Yao, J.; Cui, G. Nitrogen-doped graphene nanosheets with excellent lithium storage properties. *J. Mater. Chem.* **2011**, *21* (14), 5430−5434.
(68) Liers, C.; Aranda, E.; Strittmatter, E.; Piontek, K.; Plattner, D. A.; Zorn, H.; Ullrich, R.; Hofrichter, M. Phenol oxidation by DyP-type peroxidases in comparison to fungal and plant peroxidases. *J. Mol. Catal. B: Enzym.* **2014**, *103*, 41−46.
(69) Duan, X. G.; Sun, H. Q.; Kang, J.; Wang, Y. X.; Indrawirawan, S.; Wang, S. B. Insights into heterogeneous catalysis of persulfate activation on dimensional-structured nanocarbons. *ACS Catal.* **2015**, *5* (8), 4629−4636.
(70) Lee, H.; Lee, H.-J.; Jeong, J.; Lee, J.; Park, N.-B.; Lee, C. Activation of persulfates by carbon nanotubes: Oxidation of organic compounds by nonradical mechanism. *Chem. Eng. J.* **2015**, *266*, 28−33.
(71) Wang, X. B.; Qin, Y. L.; Zhu, L. H.; Tang, H. Q. Nitrogen-doped reduced graphene oxide as a bifunctional material for removing bisphenols: synergistic effect between adsorption and catalysis. *Environ. Sci. Technol.* **2015**, *49* (11), 6855−6864.
(72) Lei, H.; Snyder, S. A. 3D QSPR models for the removal of trace organic contaminants by ozone and free chlorine. *Water Res.* **2007**, *41* (18), 4051−4060.
(73) Ye, T.; Wei, Z.; Spinney, R.; Dionysiou, D. D.; Luo, S.; Chai, L.; Yang, Z.; Xiao, R. Quantitative structure−activity relationship for the apparent rate constants of aromatic contaminants oxidized by ferrate (VI). *Chem. Eng. J.* **2017**, *317*, 258−266.
(74) Xiao, R.; Ye, T.; Wei, Z.; Luo, S.; Yang, Z.; Spinney, R. Quantitative structure−activity relationship (QSAR) for the oxidation of trace organic contaminants by sulfate radical. *Environ. Sci. Technol.* **2015**, *49* (22), 13394−13402.
(75) Xiao, R.; Zammit, I.; Wei, Z.; Hu, W. P.; MacLeod, M.; Spinney, R. Kinetics and mechanism of the oxidation of cyclic methylsiloxanes by hydroxyl radical in the gas phase: An experimental and theoretical study. *Environ. Sci. Technol.* **2015**, *49* (22), 13322−13330.

DOI: 10.1021/acs.est.7b03014
Environ. Sci. Technol. 2017, 51, 11288−11296

(76) Li, X.; Zhao, W.; Li, J.; Jiang, J.; Chen, J.; Chen, J. Development of a model for predicting reaction rate constants of organic chemicals with ozone at different temperatures. *Chemosphere* **2013**, *92* (8), 1029−1034.
(77) Schindler, M. A QSAR for the prediction of rate constants for the reaction of VOCs with nitrate radicals. *Chemosphere* **2016**, *154*, 23−33.
(78) Luo, S.; Wei, Z.; Dionysiou, D. D.; Spinney, R.; Hu, W.-P.; Chai, L.; Yang, Z.; Ye, T.; Xiao, R. Mechanistic insight into reactivity of sulfate radical with aromatic contaminants through single-electron transfer pathway. *Chem. Eng. J.* **2017**, *327*, 1056−1065.
(79) Mahdi Ahmed, M.; Barbati, S.; Doumenq, P.; Chiron, S. Sulfate radical anion oxidation of diclofenac and sulfamethoxazole for water decontamination. *Chem. Eng. J.* **2012**, *197* (14), 440−447.

DOI: 10.1021/acs.est.7b03014
Environ. Sci. Technol. 2017, 51, 11288−11296